Article

Towards Multi-Scale Space-Time Characteristics of Air Quality and Population Exposure Risk

Xiao Xiao [1,2], **Xiao Xie [1,3],***, **Bingyu Zhao [1,2]**, **Jingzhong Li [3,4]** and **Bing Xue [1,3]**

[1]   Key Lab for Environmental Computation and Sustainability of Liaoning Province, Institute of Applied Ecology, Chinese Academy of Sciences, Shenyang 110016, China; xiaoxiao@iae.ac.cn (X.X.); zhaobingyu0@163.com (B.Z.); xuebing@iae.ac.cn (B.X.)

[2]   University of Chinese Academy of Sciences, Beijing 100049, China

[3]   Weifang Institute of Modern Agriculture and Ecological Environment, Weifang 261041, China; zhong_lij@163.com

[4]   College of Urban Planning and Architecture, Xuchang University, Xuchang 461000, China

*   Correspondence: xiexiao@iae.ac.cn

Abstract: In order to formulate policies to control regional air pollution and promote sustainable human–land system development, it is crucial to study the space–time distribution of air pollution and the population exposure risk. Existing studies are limited to individual fine particulate pollutants, which does not fully reflect the comprehensiveness of air quality. In addition, the spatiotemporal distribution of air quality and population exposure risk at different scales need to be further quantified. In this study, we used air monitoring station data and population spatial distribution data to analyze the spatiotemporal characteristics of air quality, including seasonal variations, variations before and during heating periods, and the occurrence frequency of priority pollutants in the traditional industrial areas of Northeast China in 2015. The population exposure–air pollution risk (PE-APR) model was used to calculate the population exposure risk at different spatial scales. The results suggest that GIS methods and air monitoring data help to establish a comprehensive air quality analysis framework, revealing spring–summer differentiation and the change trend of air quality with latitude. There are significant clustering features of air quality. A grid-scale population exposure–air pollution risk map is not restricted by administrative boundaries, which helps to discover high-risk areas of the main regional economic corridors and differences between inner cities and suburbs. This study provides a reference for understanding the space–time evolution of regional air pollution and formulating coordinated cross-regional air pollution strategies.

Keywords: human–land relationship; air quality; population exposure–air pollution risk; spatial autocorrelation; traditional industrial areas of Northeast China

1. Introduction

Air pollution is an essential factor that affects populations in cities and industrial regions [1]. For example, the smog in China at the beginning of 2013 affected more than 8 million people, causing global concern [2]. Affected by natural geomorphology and economic structure [3], air pollution has a significant impact on human health, such as the development of respiratory and cardiovascular diseases [4,5]. In the past decade, China has successfully formulated a series of policies on energy conservation, emission reduction [6] and atmospheric environmental governance [7]. Air quality has improved since the policies were implemented. However, under the guidance of the Sustainable Development Goals, the temporal and spatial distribution of regional air pollution, the temporal and spatial variation of pollutants [8], and the threat to human health need to be further clarified [9], in order to formulate and promote regional environmental governance policies [10].

At present, studies on the spatiotemporal distribution and visualization of air pollution mainly focus on the concentrations of atmospheric pollutants, looking at single pollutants at different spatial scales or multiple contaminants [11]. Some studies have also investigated

the spatiotemporal changes of air pollution in the country [12], urban cluster [13], city [14], and community scale in China [15]. For example, Liu et al. used spatial autocorrelation analysis and three spatial measurement models to analyze the temporal and spatial characteristics of $PM_{2.5}$ in the Beijing–Tianjin–Hebei region [16]. Another study found that the air quality in megacities such as Beijing and Shanghai has noticeable seasonal changes, and the pollution sources are increasingly complex [14]. Since the average air quality index of a single administrative unit cannot reveal the continuous microscopic changes in air pollution concentrations on a region scale, remote sensing data such as aerosol optical depth, have gradually been integrated and applied. For example, one study [17] explained the spatial and temporal distribution characteristics of critical pollutants in China from 1999–2011 by conducting a human health risk assessment of $PM_{2.5}$ based on time series of $PM_{2.5}$ concentrations obtained by remote sensing. The research conclusions may have been biased due to the uncertainty caused by spatial resolution, meteorology and topography [18].

In terms of assessing the population exposure risk of air pollution, existing studies mainly focus on fine particle pollutants such as $PM_{2.5}$ and PM_{10} [19,20]. However, health risk should not be viewed simply as an individual pollutant concentration issue. On the contrary, pollutants have a collective or synergistic effect on health risk [21]. Researchers have focused on two air pollutant exposure assessment methods: one is to quantify exposure by determining the concentration of air pollutants released into the environment, and the other is an air pollution exposure model that takes into account the characteristics of population distribution. The latter was proven to have higher accuracy and theoretical reliability in estimating air pollution exposure [22].

In order to improve the accuracy of population distribution, population spatial distribution data were developed from the average population density of a certain administrative level spatial unit to high-resolution population grid data [23]. In addition, the traditional air pollution exposure model that takes into account population distribution can theoretically obtain relatively high-precision exposure assessment results for each spatial unit [24], but the incomparability of the risk values among the units limits the application of this model to larger geographic areas [25,26]. The recently proposed "population weighted exposure risk model" is considered to be able to distinguish the severity of air pollution exposure in a certain spatial unit relative to that within the overall spatial unit [27]. This model has potential value for revealing the spatial distribution characteristics of exposure risk in large geographic areas at different scales. GIS enables the visualization of human–land elements in multi-scale geographic units [28,29] and shows certain advantages in the study of human–land coupling relationships [30–32]. In recent years, more and more studies have discovered the potential of GIS tools in air pollution exposure assessment research. GIS not only converts pollution detection points into a continuous surface but also provides a way to combine pollutant and population data on multiple scales, providing explicit tools for assessing exposure [21–23]. Therefore, conducting a study on the spatiotemporal distribution of regional multi-level air pollution and assessing the population exposure risk by GIS spatial analysis methods is crucial to better understand the complexity of urban air governance and promote refined "people-oriented" environmental governance.

Northeast China is a typical traditional industrial area in China and worldwide [33], including 36 cities in the three provinces of Liaoning, Jilin, and Heilongjiang. The latitude and longitude of Northeast China range from 120° E to 135° E and 38° N to 56° N. The area has typical regional characteristics [34]. As a traditional old industrial base and an important agricultural base, the region has diverse air pollution emission sources. The terrain is not conducive to the diffusion and transmission of atmospheric pollutants. The main atmospheric transmission channel is the heavy smog-polluted Beijing–Tianjin–Hebei region, and the long-distance transmission of pollutants may affect the air quality in this area. Most of the cities in Northeast China have a temperate monsoon climate with warm summers and long winters [35]. Due to the cold weather in autumn and winter and the influence of heating, air pollution incidents occur from time to time, which has attracted great attention [36]. However, studies on air pollution in the region have been limited to

Changchun City [37], Suihua City [38] and other cities, focusing on pollutants related to rural straw burning, such as $PM_{2.5}$ and CO [39]. Therefore, based on the air monitoring station data and population distribution data of 36 cities in Northeast China, this study used GIS spatial interpolation and spatial autocorrelation analysis to quantitatively reveal the spatiotemporal characteristics of the region, in order to provide a scientific basis for further exploration of the driving mechanisms of air pollution. In addition, we adopted a population-weighted air pollution exposure risk assessment model to assess people's exposure risk at different spatial scales, and our results provide decision-making support for the formulation of environmental governance policies in regions, cities, and central urban areas.

2. Materials and Methods

2.1. Data Collection and Processing

The daily air quality data of 36 environmental monitoring sites in Northeast China from 1 January to 31 December 2015, were obtained from the Data Centre of the Ministry of Environmental Protection (now Ministry of Ecology and Environment) (http://www.mee.gov.cn/, accessed on 19 September 2016). The daily air quality data include daily Air Quality Index (*AQI*), air quality, and priority pollutants values. When the instrument needs maintenance or communication failure occurs, sites may have no data for a period. For example, there were no data at all on 18 April and 24 August 2015. When the air quality level is "excellent", there is no priority pollutant information. The daily air quality data were calculated according to the results of the national air quality automatic monitoring stations in accordance with the Ambient Air Quality Index Technical Regulations (Trial) (HJ633-2012) [40]. Among them, *AQI* is a dimensionless index that quantitatively describes and comprehensively reflects air quality status. The regional *AQI* takes the maximum value of the Individual Air Pollutant Index (IAQI), which is calculated based on the measured concentrations of individual pollutants including fine particulate matter, inhalable particulate matter, sulfur dioxide, nitrogen dioxide, ozone, and carbon monoxide [40]. Larger *AQI* values indicate more serious pollution and a greater impact on human health. The *AQI* is divided into six levels: level 1 (excellent, 0–50), level 2 (good, 51–100), level 3 (lightly polluted, 101–150), level 4 (moderately polluted, 151–200), level 5 (severely polluted, 201–300), and level 6 (most severely polluted, >300) [41]. A priority pollutant is one whose IAQI is the largest when *AQI* > 50 [41].

The population data of the study area include total prefecture-level administrative district population and kilometer-level grid population distribution data. The former data were obtained from the statistical yearbooks of various administrative districts in the study area, while the latter were obtained from the "population spatial distribution kilometer grid data set" [42] of the Resource and Environmental Science Data Centre of the Chinese Academy of Sciences. The latter data reflect detailed population spatial distribution. We clipped the population distribution data using the boundary data of the study area. The population distribution data were re-projected to the CGCS2000 coordinate system.

Our data processing steps included the following: (1) We calculated the number of days at each air quality level in the year and then calculated the number of days at each air quality level in each season. Here, according to the seasonal division of Northeast China in the existing studies [43], we defined spring as March to May, summer as June to August, autumn as September to November, and winter as December to February. (2) We calculated the average value of the daily *AQI* of monitoring stations in the four seasons, excluding periods without data. The spatial interpolation method was then used to calculate the *AQI* value around the monitoring stations, and ArcGIS 10.2 was used to draw a continuous spatial distribution map of the *AQI* in each season. (3) According to the *AQI* spatial distribution data obtained in step 2, we used ArcGIS 10.2 to obtain the average *AQI* value of each city. Taking the *AQI* of each city as the input variable, we carried out spatial autocorrelation analysis. (4) We calculated the average number of days when priority pollutants appeared at 36 monitoring sites in each month, then drew a histogram of

their monthly changes in the entire study area. (5) According to the *AQI* spatial distribution data obtained in step 2, we used ArcGIS 10.2 to obtain the average *AQI* of each grid of the 1 km × 1 km -resolution population data. Then we used the population exposure–air pollution risk assessment model to calculate the air pollution exposure risk at the city and grid scale.

2.2. Methods

2.2.1. Spatial Interpolation Method

As the measured *AQI* data are in the form of discrete points, the continuous spatially distributed data values can be estimated by a spatial interpolation method [44]. Inverse distance weight interpolation is based on the principle of similarity: the closer the distance between two objects (such as Euclidean distance), the stronger the similarity of their properties [45,46]. The Euclidean distance between P_i and P_j is calculated with the following equation:

$$D_{ij} = \sqrt{(x_j - x_i)^2 + (y_j - y_i)^2}$$ (1)

where x_i and y_i represent the coordinates of point P_i, and x_j and y_j represent the coordinates of point P_j. D_{ij} represents the Euclidean distance between points P_i and P_j.

P_j represents the interpolation point and P_i represents the known sample point; the attribute value of the known point P_i is Z_i; and the calculation formula for attribute value Z_j of point P_j is shown in Equation (2):

$$Z_j = \sum_{i=1}^{n} (w_{ij} Z_i)$$ (2)

where w_{ij} represents the weight matrix, which is inversely proportional to the distance d_{ij} from P_j to the known points around.

2.2.2. Spatial Autocorrelation Analysis

In order to quantitatively measure the correlation of air quality between cities and further reveal its regional characteristics, this study used the global Moran's I spatial autocorrelation index and local Getis-Ord G_i^* to measure the spatial autocorrelation of urban air quality.

(1) Global Moran's I is a statistic that describes the average degree of correlation between all spatial units and the surrounding area over the entire area [47]. The calculation formula is as follows:

$$I = \frac{k \sum_{i=1}^{k} \sum_{j=1}^{k} W_{ij}(x_i - \bar{x})(x_j - \bar{x})}{\sum_{i=1}^{k} \sum_{j=1}^{k} W_{ij} \sum_{i=1}^{k}(x_i - \bar{x})^2}$$ (3)

where $\bar{x}$ is the mean value of observations at all k locations (regions), W_{ij} is the spatial weight matrix, x_i and x_j are the observations at spatial locations i and j. The range of I is [–1, 1]. If I is −1, the observations have complete negative correlations in space; if I is 1, the observations have complete positive correlation in space; if I is 0, the observations are not correlated. The significance of the spatial autocorrelation of the study unit is tested using the standardized statistic Z as follows:

$$Z = \frac{I - E(I)}{\sqrt{VAR(I)}}$$ (4)

where $E(I)$ is the expectation of I and $VAR(I)$ is the variance of I. When the Z value is positive and significant ($Z > 1.96$), it indicates a positive spatial autocorrelation, that is, similar observations (high or low value) tend to be spatially clustered. When the Z value is negative and significant ($Z < −1.96$), there is a negative spatial autocorrelation, and similar observations tend to be distributed. When $Z = 0$, the observations are independent and

random. Utilizing the GIS regional statistics method to calculate the average *AQI* for each city, we analyzed the global spatial autocorrelation of *AQI* at a prefecture scale.

(2) The hot spot analysis tool (Getis-Ord G_i^*) [48] detects high-value clusters and low-value clusters based on the local spatial autocorrelation index of the distance weight matrix. The local spatial autocorrelation index G_i^* is calculated with the following formula:

$$G_i^* = \frac{\sum_{j=1}^n W_{ij}(d) X_j}{\sum_{j=1}^n X_j} j \neq i \tag{5}$$

where X_j is the element attribute value of the *j*th spatial unit, *n* is the total number of elements, and W_{ij} is the spatially adjacent weight matrix within distance *d*. If the distance between the *i*th and *j*th spatial units is within the given critical distance *d*, they are considered neighbors. The element in the spatial weight matrix is 1; otherwise, the element is 0. The local spatial autocorrelation index G_i^* is standardized in Equation (6).

$$Z = \frac{(G_i^*) - E(G_i^*)}{\sqrt{Var(G_i^*)}} \tag{6}$$

where $E(G_i^*)$ is the mathematical expectation value, and $Var(G_i^*)$ is the variation coefficient. When $Z > 1.96$ and the confidence level is greater than 90% ($p < 0.1$), the value around unit *i* is relatively large, i.e., unit *i* is a significant hot spot; when $Z < -1.96$ and the confidence is greater than 90% ($p < 0.1$), it means that unit *i* is a significant cold spot. In (5), if the value of critical distance *d* is too high, it is difficult to reflect the hierarchical distribution of hot spots. If the value of critical distance *d* is too low, it is difficult to meet the statistical conditions. In order to highlight the urban-scale hot spots characteristics of air quality in Northeast China, we selected 200, 400, and 600 km as critical distances for the experiment, and finally used 400 km as the compromise fixed distance for air quality hot spot analysis.

2.2.3. *Population Exposure–Air Pollution Risk Assessing Model*

In order to distinguish the severity of air pollution exposure in a spatial subunit relative to that within the overall spatial unit, Zou et al. constructed a model for assessing the population relative risks of air pollution exposure (MAPRRAPE) [45]:

$$PRRAPE_i = \frac{P_i \times C_i \times n}{\sum_{i=1}^n P_i \times C_i} \tag{7}$$

where $PREAPE_i$ is the population relative risks of air pollution exposure in the *i*th *grid*, *i* is the number of grids, P_i is the population density of the *i*th *grid*, C_i is the concentration of an individual pollutant within the *i*th *grid*, and *n* is the total number of grids.

It is recognized that air pollution exposure risk assessment should not simply consider an individual pollutant, but instead assume that pollution is caused by multiple pollutants [21]. In order to consider the health risks caused by multiple air pollutants, we constructed a new population exposure–air pollution risk assessment model by referring to and improving MAPRRAPE. The new model is as follows:

$$PE - APR_i = \frac{P_i \times AQI_i \times n}{\sum_{i=1}^n P_i \times AQI_i} \tag{8}$$

where $PE\text{-}APR_i$ is the relative risks in the *i*th *grid*, *i* is the number of grids, P_i is the population density of the *i*th *grid*, and the unit is person/*grid*. AQI_i is the *AQI* in *grid* *i* and *n* is the total number of grids in the area. When $PE\text{-}APR_i$ is between 0 and 1, it means that the exposure level is lower than the regional average, and when $PE\text{-}APR_i > 1$, it indicates otherwise.

3. Results and Discussion

3.1. Spatial and Temporal Changes of Air Quality

The air quality level with the highest frequency in Northeast China in 2015 was level 2 (good), accounting for 24% of the total days of the year, followed by level 1 (excellent) at 53%, level 3 (lightly polluted) at 15%, level 4 (moderately polluted) at 4%, level 5 (severely polluted) at 3%, and level 6 (most severely polluted) at 1% (see Figure 1). From the perspective of seasonal distribution, the frequency of lightly polluted or worse than slightly polluted air quality was ranked in the order of winter, autumn, spring, summer, while the ranking of excellent and good levels was the opposite (Figure 2).
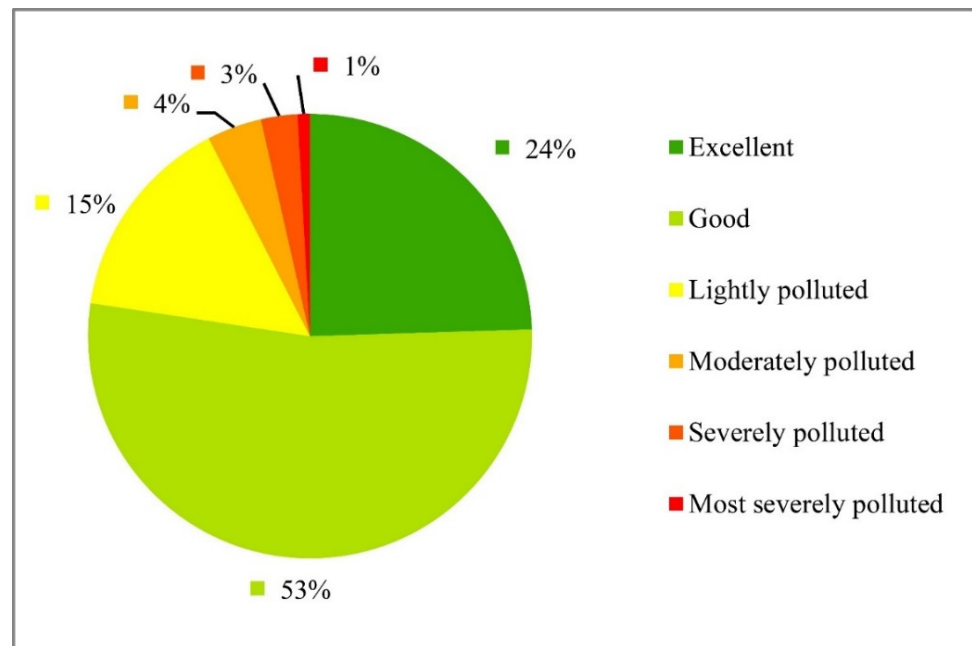

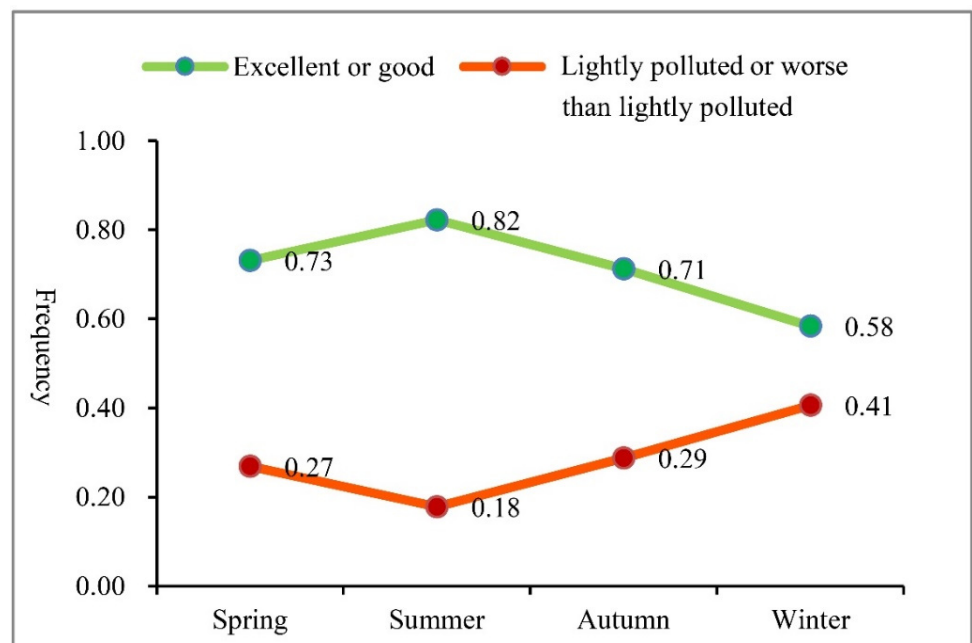**Figure 1.** Proportion of days with different levels of air quality throughout the year.

Figure 2. The frequency of air quality in each season.

The air quality in Northeast China shows typical characteristics of winter–summer differentiation. The degree of change in air quality varies with the seasons in each province. For example, the air quality of Heilongjiang Province has an *AQI* in the range of 100 in winter and summer, while the *AQI* in Liaoning Province fluctuates between 80 and 110. The *AQI* in the northern area in spring and summer shows a gradient increasing trend with decreasing latitude, while the *AQI* in autumn and winter shows characteristics of circle diffusion and attenuation, with the provincial capital as the high-value center (Figure 3). For example, in winter, the *AQI* of Harbin is the highest. From Harbin to the south, a regional circle with the worst air quality composed of Changchun, Jilin, Siping, Liaoyuan, and Fushun has formed. The *AQI* of the cities within this circle was higher than 110. The main reason is that the provincial capitals are more densely populated, and the anthropogenic emissions caused by gasoline and coal-fired heating devices have aggravated urban air pollution [49]. Moreover, illegal emissions and biomass combustion in winter are the main drivers of the formation of dense fog, which makes air pollution more serious [50].
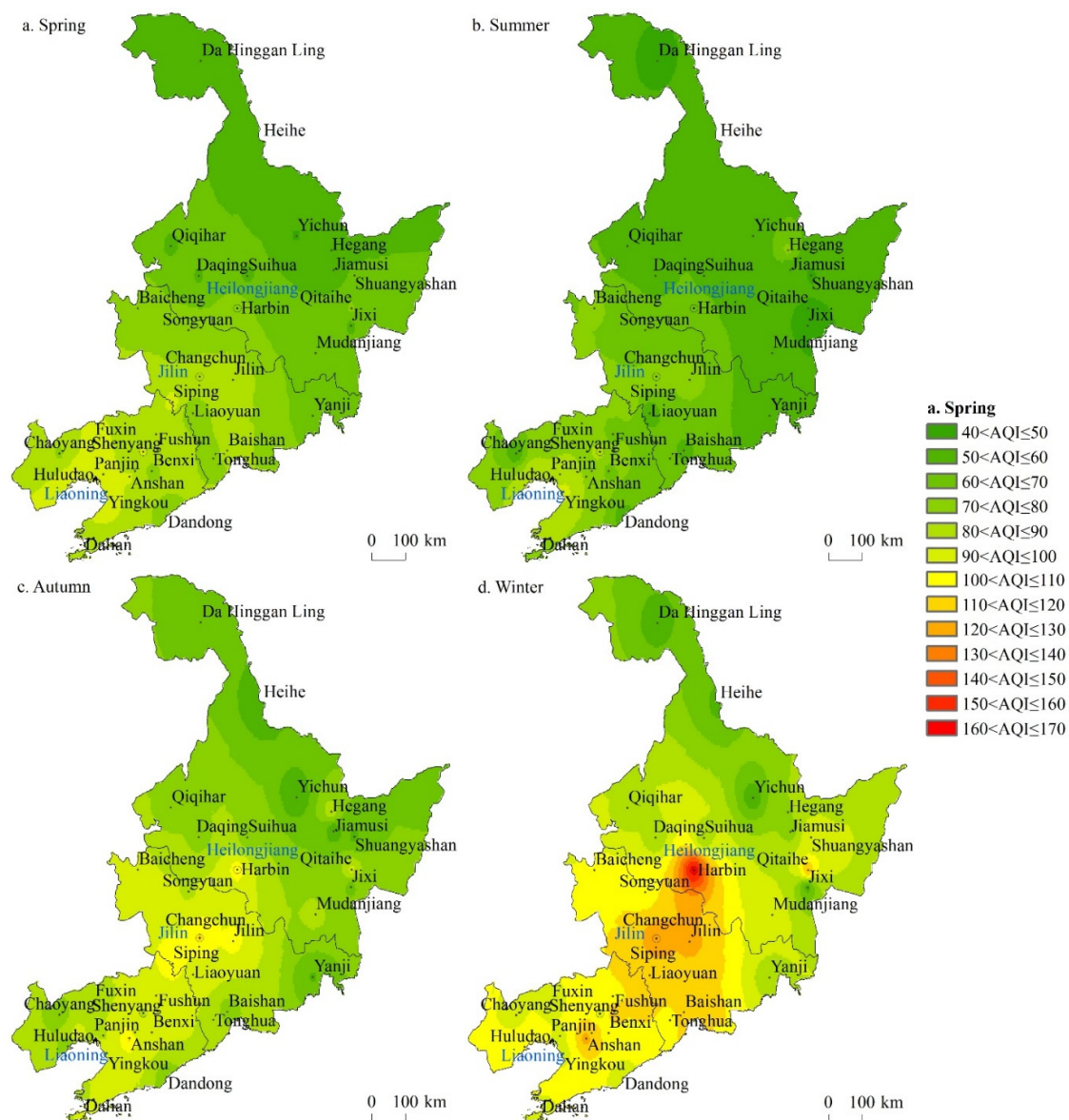

Figure 3. Spatial distribution of *AQI* in each season.

The Moran's I values of urban *AQI* were 0.71 (spring), 0.67 (summer), 0.55 (autumn), and 0.43 (winter), with corresponding Z-values of 13.61, 12.89, 10.72, and 8.48. The Z-values

were greater than 1.65 with a confidence level above 90%, indicating that a significant positive spatial autocorrelation of *AQI* in the four seasons with a significant spatial agglomeration pattern. The Getis-Ord G_i^* of *AQI* indicates that the average urban *AQI* conforms to the statistical characteristics of the hot spot analysis clustering mode. Visually expressing the Z-value, it is concluded that significant hot spots with Z > 1.96 and *p* < 0.05 are mainly distributed in Liaoning and Jilin Provinces (Figure 4). The distribution of significant *AQI* hot spots in these two provinces is concentrated; they are mainly located in Liaoning in spring and summer, and move northward in autumn and winter, covering the central area of the two provinces. Significant hot spot cities have higher *AQI* values and are surrounded by neighboring cities that also have high values, which means that they are statistically high *AQI* cluster areas. In winter, Harbin City in Heilongjiang Province was shown to have a high *AQI* value, but there were no significant hot spots surrounded by other cities with high *AQI*.
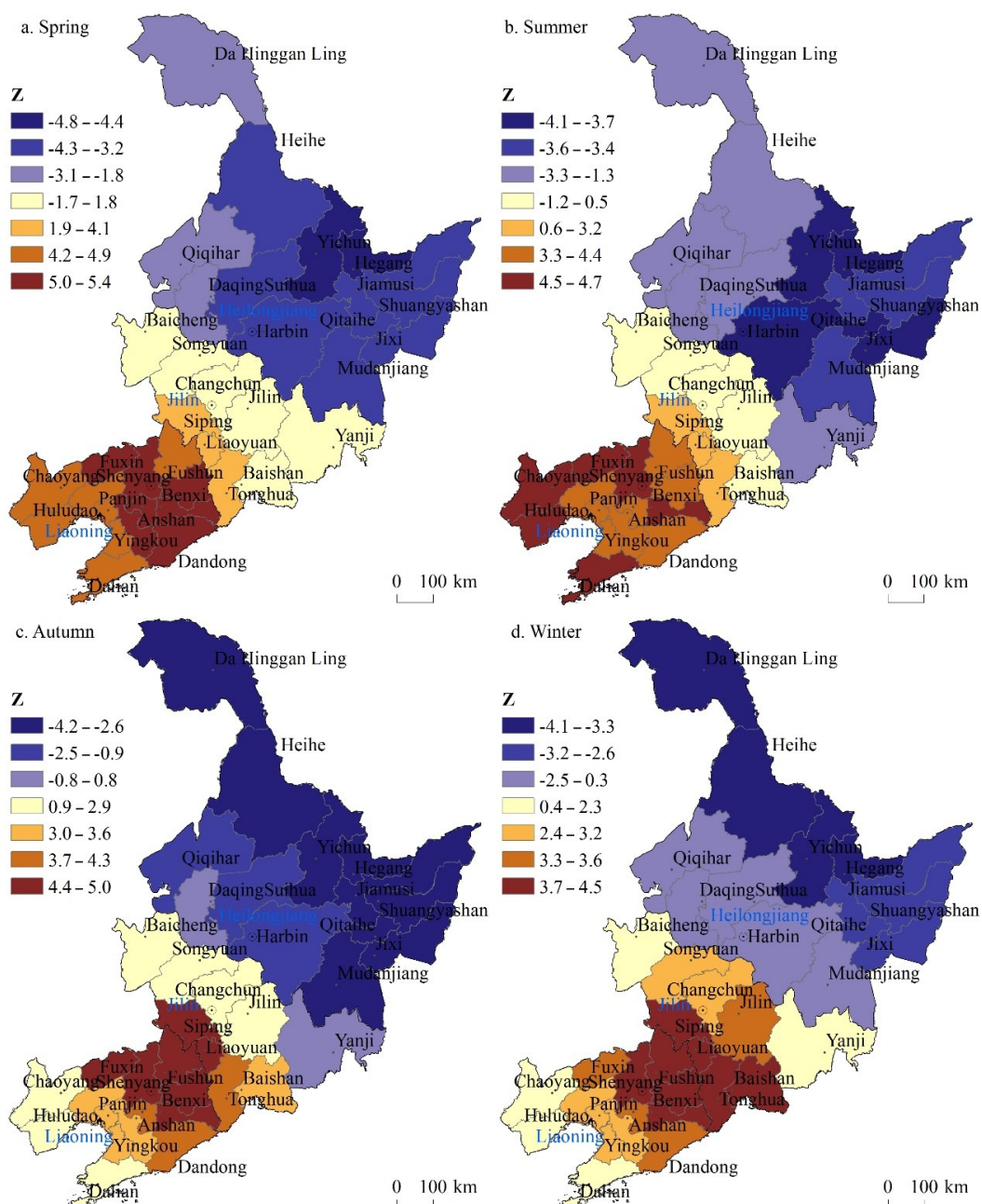

Figure 4. Spatial distribution of hot and cold spots of *AQI* in each season at urban scale.

Seasonal changes in priority pollutants in Northeast China were significant. In autumn and winter, $PM_{2.5}$ became the priority pollutant on most days, with a cumulative occurrence of 120 days, accounting for one-third of the year. PM_{10} was the priority pollutant on 77 days. The month when the highest number of days PM_{10} became the primary pollutant was April, with a total of 10 days, mainly because the wind and sand were more serious in spring than in other seasons. Sand and dust on the ground were blown by the wind transported from upstream to the local area, causing increased concentrations of PM_{10} and other atmospheric particulates [51]. O_3 was the priority pollutant on 73 days of the year. Its monthly change pattern was contrary to $PM_{2.5}$, showing an inverted U-shaped distribution pattern. The urban thermal environment in summer increases the risk of air pollution [52]. SO_2 appeared as the priority pollutant on the fewest days, only eight days of the year (Figure 5). The changes in the frequency of primary pollutants throughout the year indicate that the heating period (November through March) is a critical period for air pollution control in Northeast China.
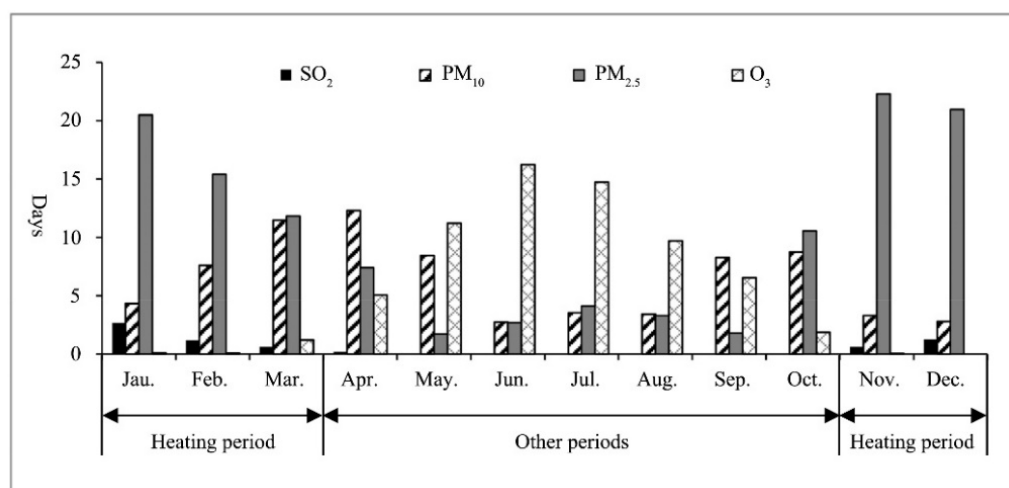

Figure 5. Changes in the frequency of priority pollutants throughout the year.

3.2. Spatial Distribution of Population Exposure–Air Pollution Risk

The population exposure–air pollution risk was characterized by high spatial differentiation in provincial capital cities and low in non-provincial capital cities (Figure 6). The PE-APR in provincial capital cities was greater than 2, among which Harbin had the highest risk (PE-APR > 3.0). The PE-APR in Dalian, Suihua, Qiqihar, Jilin, and other cities was also relatively high (PE-APR > 1). Overall, 61% of cities had a risk level lower than the regional average (0.5 < PE-APR ≤ 1). The lowest population exposure–air pollution risk area (0.1 < PE-APR ≤ 0.5) was concentrated in northern Heilongjiang, especially Da Hinggan Ling Prefecture, Qitaihe City, and Yichun City, mainly due to the good air quality throughout the year and the sparse population there. The cities with high PE-APR (2.5 < PE-APR ≤ 3.5) were Harbin, Changchun, and Shenyang; the cities with intermediate PE-APR (1.5 < PE-APR ≤ 2.5) were ranked as autumn/winter, summer, and spring.

PE-APR was divided into five levels on a grid scale: level 1 (0–1), level 2 (2–30), level 3 (31–100), level 4 (101–250), and level 5 (251–420). PE-APR changed significantly during the four seasons. Level 1 indicates that air pollution exposure levels in the area are relatively lower than or equal to the average level of the entire study area. The grid number of level 1 in descending order corresponded to summer, spring, autumn, and winter. Level 2 and above indicate that air pollution exposure levels in the area are higher than the average level for the entire study area. The grids of levels 2–5 are mainly located on the central axis connecting Harbin, Changchun, Shenyang, and Dalian, forming a belt-shaped area along the Harbin–Dalian Railway, and multiple scattered points in cities at various levels (Figure 7). This area cuts through the central region of the three northeastern provinces,

starting from central Heilongjiang Province and reaching southernmost Liaoning Province, covering the four major urban clusters: the Harbin–Dalian–Qiqihaer Economic Zone, the Changchun–Jilin–Tumen River Pilot Zone, the Liaoning Coastal Economic Belt, and the Shenyang Economic Zone. Figure 6 shows that areas with PE-APR greater than 1 are not significantly distributed around the Harbin–Dalian Railway and do not reflect the scattered points of prefectural cities. Figure 7 shows that the PE-APR of provincial capital cities is above level 3, and the central urban area within a 10 km radius is characterized by circles of decreasing levels. Therefore, the grid-scale map can show the temporal and spatial characteristics of PE-APR between and within cities in a more detailed manner.
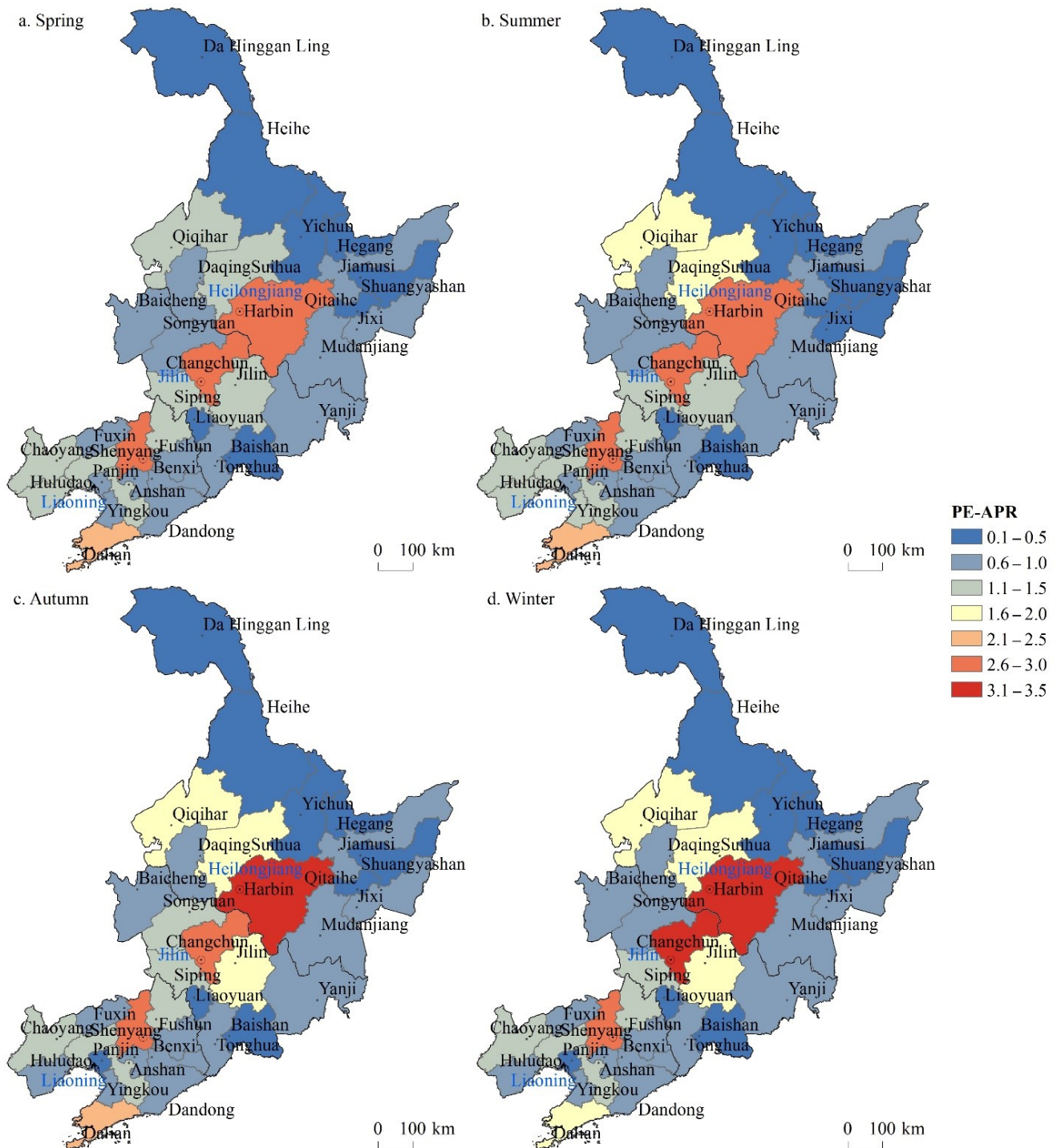

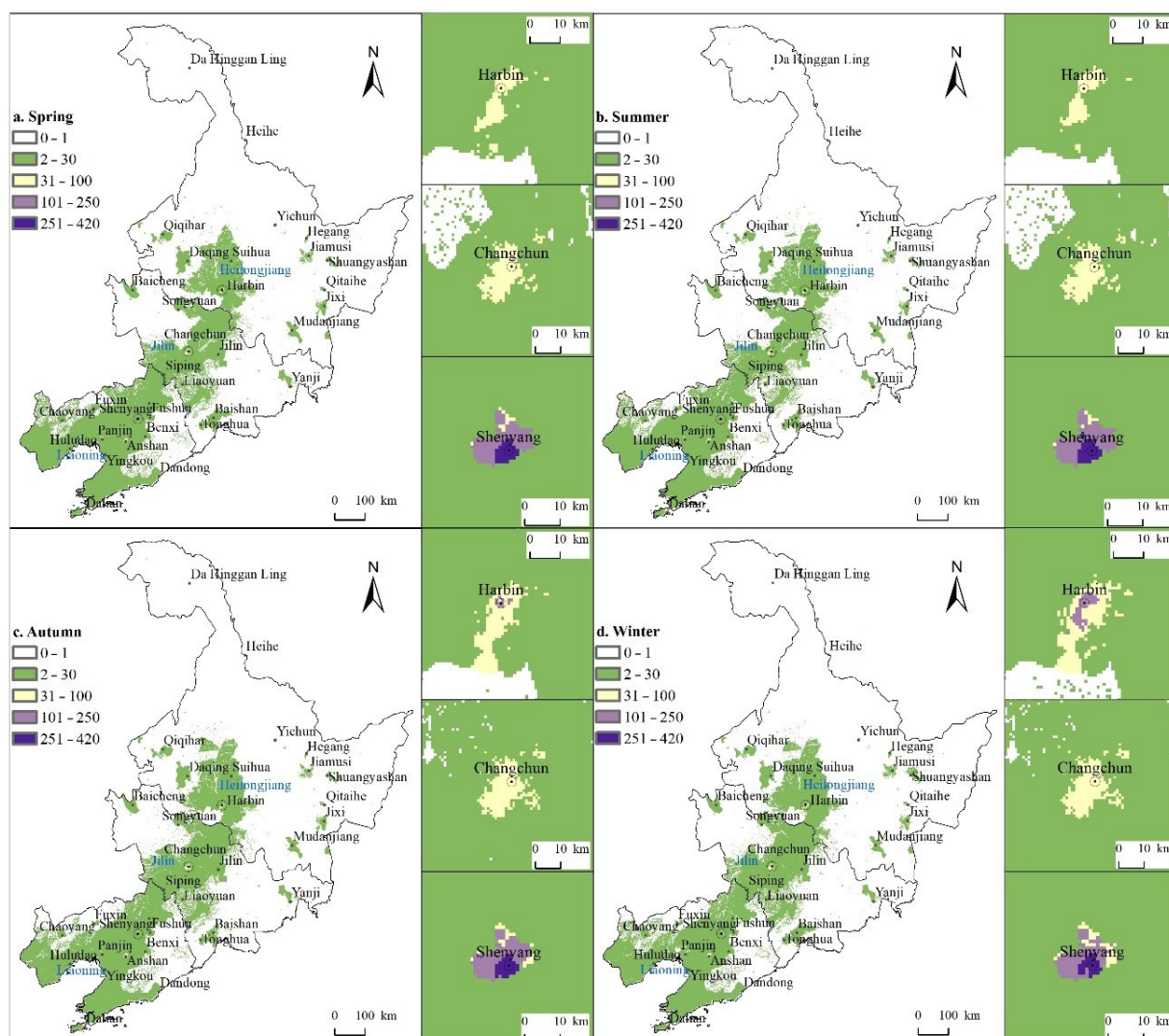**Figure 6.** Distribution of PE-APR in each season at urban scale.

Figure 7. Distribution of PE-APR in each season at grid scale.

4. Conclusions

This study constructed an integration method consisting of multiscale population data, GIS spatial interpolation methods, spatial autocorrelation analysis, and a population exposure–air pollution risk assessment model to analyze multi-scale air quality space-time characterization and population exposure risk. This method supplements the methodological system of air quality research. Compared with city-scale population data, the 1 km × 1 km resolution grid-scale population data are not restricted by administrative boundaries, which helps to detect spatial heterogeneity characteristics of air pollution exposure risk in small areas within a city [53]. The global spatial autocorrelation and hot spot analysis of urban *AQI*s help to discover regional commonalities and aggregations of *AQI*, providing a reference for further exploration of the formation mechanism of air pollution and formulation of coordinated regional measures.

Unlike previous studies that selected a few industrial, agricultural, and provincial capital cities of Northeast China as case areas [54,55], this study, selected the whole area of Northeast China as the study area, which supplements the empirical studies on regional air quality. Besides, compared with previous studies that only considered air quality changes from a single perspective (such as pollutant concentration), this study investigated the space–time characteristics of air quality from multiple perspectives, including throughout a year and a season, and the monthly change characteristics of priority pollutants.

This study found gradually decreasing air quality in Northeast China in autumn and winter, with the provincial capital city showing the highest values. The urban cluster along the Harbin–Changchun axis was found to be a key air pollution area. The results of spatial autocorrelation analysis indicate that the air quality of cities in Liaoning and Jilin Provinces had spatial correlation characteristics. The above results indicate that air pollution in Northeast China has regional characteristics. It was found that the main emission sources in Northeast China are seasonal, with contributions from crop residue combustion in autumn and winter, coal combustion in winter, and dust in spring. Therefore, in order to solve the air pollution problem in the northeast, it is urgent to formulate policies to comprehensively control coal combustion, fuel consumption, and crop residue combustion in autumn and winter. Recent "coal-to-gas" projects, clean energy substitution projects, and energy-saving measures in related industries will have a positive effect on air pollution in Northeast China. Joint air pollution prevention and control policies must be combined across regions [43]. It is necessary to establish a coordinated control mechanism for straw-burning pollution. By using a unified meteorological diffusion model and deduction method, the entire region is expected to realize information exchange, share analysis and judgment results, and carry out joint prevention and control strategies to ensure continuous improvement of regional air quality.

The exposure risk of air pollutants shows that the central area of a city is a high-risk area at the city scale, and the area along the Harbin–Dalian Economic Axis is a high exposure risk area within the region. According to Equation (8), the value of *PE-APR* is related to two parameters, AQI_i (*AQI* in the *i*-th *grid*) and P_i (population density of the *i*-th *grid*). PE-APR is positively correlated with both AQI_i and P_i, its value depends on which parameter is more dominant. The population density of the grids and cities along the Harbin–Dalian Economic Axis is much higher than that of other areas, and its impact is far stronger than *AQI*, making these grids and cities high-value areas of population exposure–air pollution risk. However, this does not mean that areas with high *PE-APR* necessarily have more severe air pollution. For example, Shenyang City has better air quality throughout the year, but it has a higher risk of air pollution exposure due to higher population density. The situation is the same in Changsha [53], where there is also a mismatch between the air pollutant concentration and population spatial distribution characteristics. However, there is a study showing that areas with severe air pollution are also areas with high population density in Lanzhou [23]. In addition, downtown areas are prone to becoming high air pollution population exposure risk areas, which was confirmed in a study in Dallas, Texas, USA [45].

The area along the Harbin–Dalian Economic Axis has a relatively high level of social and economic development, and the terrain is conducive to population gathering. In addition, a relatively complete level of social infrastructure has become the main driving factor for population migration [56]. Higher population density means that the emission potential of transportation, industry, and residents, other important causes of air pollution, is high. Therefore, central urban areas and areas such as the regional economic axis should speed up high-quality economic development with fewer resources, lower energy consumption, and less environmental damage.

Finally, we would like to note that, in our study, we used the *AQI* data of 36 monitoring sites to transform fixed-point data into continuous surfaces through GIS interpolation technology. There are unavoidable errors in the *AQI* values of areas without observational data. Using more monitoring points and an air pollution model that simulates pollutant concentrations would be effective means to reduce this deviation [57]. Moreover, different spatial interpolation methods will affect the accuracy of the *AQI*. In the future, a cross-validation scheme for interpolation accuracy based on sampling data should be designed for different spatial interpolation methods, to determine the method most suitable for air quality simulation in the study area. The European ATMOSPHERE project addresses the issue of exposure model selection [23]. Furthermore, it is difficult for one year of AQI data to reflect the long-term trend of air quality, thus collecting panel data of long-term

AQI series will be a key task in the next phase of our study. Moreover, it is necessary to use multi-source spatiotemporal big data to mine the natural/human driving factors and internal/external regional factors of air quality spatial distribution [11]. With multi-scale population data, this study distinguishes the air pollution exposure risks throughout the study area. However, the impact of human activity patterns (e.g., inhalation rate, duration of exposure) on exposure risk has not been considered. With the support of GIS, a more realistic exposure model that takes into account people's time–activity patterns can be developed in the future to assess the exposure risks of different groups.

Author Contributions: Conceptualisation, X.X. (Xiao Xiao), X.X. (Xiao Xie); data curation, X.X. (Xiao Xiao), B.Z. methodology, X.X. (Xiao Xiao)., B.Z., J.L.; formal analysis, X.X. (Xiao Xiao), X.X. (Xiao Xiao); writing—original draft preparation, X.X. (Xiao Xiao), X.X. (Xiao Xie); writing—review and editing, X.X. (Xiao Xie); visualization, X.X. (Xiao Xiao), X.X. (Xiao Xie); supervision, B.X.; project administration, B.X.; funding acquisition, B.X. All authors have read and agreed to the published version of the manuscript.

Institutional Review Board Statement: Not applicable.

Informed Consent Statement: Not applicable.

Data Availability Statement: Data available on request due to ethical restrictions. The data presented in this study are available on request from the corresponding author. The data are not publicly available due to not having participants consent to share their anonymized data with a third party.

Conflicts of Interest: The authors declare no conflict of interest. The funders had no role in the design of the study; in the collection, analyses, or interpretation of data; in the writing of the manuscript, or in the decision to publish the results.

References

1. Xue, B.; Butler, T.; Ren, W.; Zhang, Z.; Wang, Y.; Mu, Z. Reviewing Air Pollution and Public Health in China. *Eng. Sustain.* **2018**, *171*, 358–367. [CrossRef]
2. Huang, R.; Zhang, Y.; Bozzetti, C.; Ho, K.; Cao, J.; Han, Y.; Daellenbach, K.R.; Slowik, J.K.; Platt, S.M.; Canonaco, F.; et al. High Secondary Aerosol Contribution to Particulate Pollution During Haze Events in China. *Nature* **2014**, *514*, 218–222. [CrossRef] [PubMed]
3. Bai, C. Progress and Prospect on Atmospheric Haze Research in Chinese Academy of Sciences. *Bull. Chin. Acad. Sci.* **2014**, *29*, 275–281. (In Chinese) [CrossRef]
4. Andersen, Z.J.; Pedersen, M.; Weinmayr, G.; Stafoggia, M.; Galassi, C.; Jørgensen, J.T.; Sommar, J.N.; Forsberg, B.; Olsson, D.; Oftedal, B. Long-term Exposure to Ambient Air Pollution and Incidence of Brain Tumor, The European study of cohorts for air pollution effects (ESCAPE). *Neuro Oncol.* **2018**, *20*, 420–432. [CrossRef]
5. Yoo, E.H.; Brown, P.; Eum, Y. Ambient Air Quality and Spatiotemporal Patterns of Cardiovascular Emergency Department Visits. *Int. J. Health Geogr.* **2018**, *17*, 18. [CrossRef] [PubMed]
6. Jiang, L.; Xue, B.; Ma, Z.; Yu, L.; Huang, B.; Chen, X. A Life-cycle Based Co-benefits Analysis of Biomass Pellet Production in China. Renew. *Energy* **2020**, *154*, 445–452. [CrossRef]
7. Shi, X.; Zheng, Y.; Lei, Y.; Xue, W.; Yan, G.; Liu, X.; Cai, B.; Tong, D.; Wang, J. Air Quality Benefits of Achieving Carbon Neutrality in China. *Sci. Total Environ.* **2021**, *795*, 148784. [CrossRef]
8. Lanzafame, R.; Monforte, P.; Patanè, G.; Strano, S. Trend Analysis of Air Quality Index in Catania from 2010 to 2014. *Energy Procedia* **2015**, *82*, 708–715. [CrossRef]
9. Zhu, C.; Fan, R.; Sun, J.; Luo, M.; Zhang, Y. Exploring the Fluctuant Transmission Characteristics of Air Quality Index Based on Time Series Network Model. *Ecol. Indic.* **2020**, *108*, 105681. [CrossRef]
10. Yuan, Z.; Tan, Y.; Shi, F. Does Reducing Air Pollution Improve the Progress of Sustainable Development in China. *J. Clean Prod.* **2020**, *272*, 122759. [CrossRef]
11. Chattopadhyay, S.; Gupta, S.; Saha, R.N. Spatial and Temporal Variation of Urban Air Quality, A GIS approach. *J. Environ. Protect.* **2010**, *1*, 264–277. [CrossRef]

12. Lin, X.; Wang, D. Spatiotemporal Evolution of Urban Air Quality and Socioeconomic Driving Forces in China. *J. Geogr. Sci.* **2016**, *26*, 1533–1549. [CrossRef]

13. Hu, J.; Wang, Y.; Ying, Q.; Zhang, H. Spatial and Temporal Variability of $PM_{2.5}$ and PM_{10} Over the North China Plain and the Yangtze River Delta, China. *Atmos. Environ.* **2014**, *95*, 598–609. [CrossRef]

14. Ren, W.; Xue, B.; Zhang, L.; Ma, Z.; Geng, Y. Spatiotemporal Variations of Air Pollution Index in China's Megacities. *Chin. J. Ecol.* **2013**, *32*, 2788–2796. (In Chinese) [CrossRef]

15. Patton, A.P.; Perkins, J.; Zamore, W.; Levy, J.I.; Brugge, D.; Durant, J.L. Spatial and Temporal Differences in Traffic-related Air Pollution in Three Urban Neighbourhoods Near an Interstate Highway. *Atmos. Environ.* **2014**, *99*, 309–321. [CrossRef] [PubMed]

16. Liu, H.; Fang, C.; Huang, X.; Zhu, X.; Zhou, Y.; Wang, Z.; Zhang, Q. The Spatial-temporal Characteristics and Influencing Factors of Air Pollution in Beijing-Tianjin-Hebei Urban Agglomeration. *Acta Geogr. Sin.* **2018**, *73*, 177–191. (In Chinese) [CrossRef]

17. Peng, J.; Chen, S.; Lü, H.; Liu, Y.; Wu, J. Spatiotemporal Patterns of Remotely Sensed $PM_{2.5}$ Concentration in China from 1999 to 2011. *Remote Sens. Environ.* **2016**, *174*, 109–121. [CrossRef]

18. Hu, J.; Ying, Q.; Wang, Y.; Zhang, H. Characterizing Multi-pollutant Air Pollution in China, Comparison of three air quality indices. *Environ. Int.* **2015**, *84*, 17–25. [CrossRef] [PubMed]

19. Iribagiza, C.; Sharpe, T.; Coyle, J.; Nkubito, P.; Piedrahita, R.; Johnson, M.; Thomas, E.A. Evaluating the Effects of Access to Air Quality Data on Household Air Pollution and Exposure—An Interrupted Time Series Experimental Study in Rwanda. *Sustainability* **2021**, *13*, 11523. [CrossRef]

20. Habil, M.; Massey, D.D.; Taneja, A. Personal and ambient PM $_{2.5}$ exposure assessment in the city of Agra. *Data Brief* **2016**, *6*, 495–502. [CrossRef]

21. Briggs, D. The Role of Gis_Coping with Space (And Time) in Air Pollution Exposure Assessment. *J. Toxicol. Environ. Health A* **2005**, *68*, 1243–1261. [CrossRef] [PubMed]

22. Dong, X.; Zhao, X.; Peng, F.; Wang, D. Population based Air Pollution Exposure and its influence factors by Integrating Air Dispersion Modeling with GIS Spatial Analysis. *Sci. Rep.* **2020**, *10*, 479. [CrossRef]

23. Sun, Z.; An, X.; Tao, Y.; Hou, Q. Assessment of Population Exposure to PM_{10} for Respiratory Disease in Lanzhou (China) and Its Health-related Economic Costs Based on GIS. *BMC Public Health* **2013**, *13*, 891. [CrossRef]

24. Kousa, A.; Oglesby, L.; Koistinen, K.; Künzli, N.; Jantunen, M. Exposure Chain of Urban Air $PM_{2.5}$—Associations Between Ambient Fixed Site, Residential Outdoor, Indoor, Workplace and Personal Exposures in Four European Cities in the EXPOLIS-study. *Atmos. Environ.* **2002**, *36*, 3031–3039. [CrossRef]

25. Zou, B.; Wilson, J.G.; Zhan, F.B.; Zeng, Y. Spatially Differentiated and Source-specific Population Exposure to Ambient Urban Air Pollution. *Atmos. Environ.* **2009**, *43*, 3981–3988. [CrossRef]

26. Wang, S.; Zhao, Y.; Chen, G.; Wang, F.; Aunan, K.; Hao, J. Assessment of population exposure to particulate matter pollution in Chongqing, China. *Environ. Pollut.* **2008**, *153*, 247–256. [CrossRef]

27. Fu, Q.; Kan, H. Air pollution dispersion model and assessment of population weighted exposure. *J. Env. Health* **2004**, *21*, 414–416. (In Chinese) [CrossRef]

28. Xue, B.; Xiao, X.; Li, J.; Xie, X.; Lu, C. Spatio-temporal Evolution of Water Areas and Croplands in the Three Provinces of Northeast China Based on Remote Sensing Data. *Chin. J. Ecol.* **2019**, *38*, 1444–1452. (In Chinese) [CrossRef]

29. Xue, B.; Xiao, X.; Li, J. Identification Method and Empirical Study of Urban Industrial Spatial Relationship Based on POI Big Data, A Case of Shenyang City. *China Geogr. Sustain.* **2020**, *1*, 152–162. [CrossRef]

30. Xue, B.; Li, J.; Xiao, X.; Xie, X.; Pang, M.; Jiang, L.; Lu, C.; Ren, W. A Big-data-based Platform for Human-land Relations Analysis and Application in Urban Areas —The GSC best practice data computing environment 2018. *J. Glob. Chang. Data Discov.* **2018**, *2*, 179–183+290–294. (In Chinese) [CrossRef]

31. Xue, B.; Li, J.; Xiao, X.; Xie, X.; Lu, C.; Ren, W.; Jiang, L. Overview of Man-Land Relationship Research Based on POI Data, Theory, Method and Application. *Geogr. Geo-Inf. Sci.* **2019**, *35*, 51–60. (In Chinese) [CrossRef]

32. Yang, J.; Wang, Y.; Xiu, C.; Xiao, X.; Xia, J.; Jin, C. Optimizing Local Climate Zones to Mitigate Urban Heat Island Effect in Human Settlements. *J. Clean Prod.* **2020**, *275*, 123767. [CrossRef]

33. Xue, B.; Xiao, X.; Li, J.; Xie, X. Analysis of Spatial Economic Structure of Northeast China Cities Based on Points of Interest Big data. *J. China Univ. Geosci.* **2020**, *40*, 691–700. (In Chinese) [CrossRef]

34. Lu, C.; Xue, B.; Lu, C.; Wang, T.; Jiang, L.; Zhang, Z.; Ren, W. Sustainability Investigation of Resource-Based Cities in Northeastern China. *Sustainability.* **2016**, *8*, 1058. [CrossRef]

35. Jin, S.; Yang, J.; Wang, E.; Liu, J. The Influence of High-speed Rail on Ice–snow Tourism in Northeastern China. *Tour. Manag.* **2020**, *78*, 104070. [CrossRef]

36. He, Y.; Zhang, X.; Chen, W.; Zhang, S.; Zhao, H. Spatial-temporal Characteristics of Regional Air Quality in Northeastern China Based on Multi-satellites Aerosol Products. *Acta Sci. Circumstantiae* **2018**, *38*, 607–617. (In Chinese) [CrossRef]

37. Chen, W.; Tong, D.; Dan, M.; Zhang, S.; Zhang, X.; Pan, Y. Typical Atmospheric Haze During Crop Harvest Season in Northeastern China, A Case in the Changchun Region. *J. Environ. Sci.* **2017**, *54*, 101–113. [CrossRef]

38. Li, L.; Wang, K.; Chen, W.; Zhao, Q.; Liu, L.; Liu, W.; Liu, Y.; Jiang, J.; Liu, J.; Zhang, M. Atmospheric Pollution of Agriculture-oriented Cities in Northeast China, A Case in Suihua. *J. Environ. Sci.* **2020**, *97*, 85–95. [CrossRef]

39. Li, Y.; Liu, J.; Han, H.; Zhao, T.; Zhang, X.; Zhuang, B.; Wang, T.; Chen, H.; Wu, Y.; Li, M. Collective Impacts of Biomass Burning and Synoptic Weather on Surface $PM_{2.5}$ and CO in Northeast China. *Atmos. Environ.* **2019**, *213*, 64–80. [CrossRef]

40. Ministry of Environmental Protection of the People's Republic of China. Technical Regulation on Ambient Air Quality Index (on trial). 2012. Available online: http://www.mee.gov.cn/ywgz/fgbz/bz/bzwb/jcffbz/201203/t20120302_224166.shtml (accessed on 15 July 2021). (In Chinese)

41. Zhan, D.; Kwan, M.P.; Zhang, W.; Yu, X.; Meng, B.; Liu, Q. The Driving Factors of Air Quality Index in China. *J. Clean Prod.* **2018**, *197*, 1342–1351. [CrossRef]

42. Xu, X. 1 km Grid Population Dataset of China, Data Registration and Publishing System of the Resource and Environmental Science Data Center of the Chinese Academy of Sciences. 2017. Available online: https://www.resdc.cn/DOI/doi.aspx?DOIid=32 (accessed on 20 August 2021).

43. Chen, W.; Liu, Y.; Wu, X.; Bao, Q.; Gao, Z.; Zhang, X.; Zhao, H.; Zhang, S.; Xiu, A.; Cheng, T. Spatial and Temporal Characteristics of Air Quality and Cause Analysis of Heavy Pollution in Northeast China. *Environ. Sci.* **2019**, *40*, 4810–4823. (In Chinese) [CrossRef]

44. Price, D.T.; Mckenney, D.W.; Nalder, I.; Hutchinson, M.F.; Kesteven, J.L. A Comparison of Two Statistical Methods for Spatial Interpolation of Canadian Monthly Mean Climate Data. *Agric. For. Meteorol.* **2000**, *101*, 81–94. [CrossRef]

45. Zou, B.; Peng, F.; Jiao, L.; Weng, M. GIS Aided Spatial Zoning of High-resolution Population Exposure to Air Pollution. *Geomat. Inf. Sci. Wuhan Univ.* **2013**, *38*, 334–338. (In Chinese) [CrossRef]

46. Ian, A.; Nalder, R.; Wein, W. Spatial interpolation of climatic Normals, Test of a new method in the Canadian boreal forest. *Agric. For. Meteorol.* **1998**, *92*, 211–225. [CrossRef]

47. Moran, P. Notes on Continuous Stochastic Phenomena. *Biometrika* **1950**, *37*, 17–23. [CrossRef] [PubMed]

48. Ord, J.K.; Getis, A. Local Spatial Autocorrelation Statistics, Distributional Issues and An Application. *Geogr. Anal.* **1995**, *27*, 286–306. [CrossRef]

49. Hao, Y.; Meng, X.; Yu, X.; Li, M.; Li, W.; Shi, F.; Yang, W.; Zhang, S.; Xie, S. Characteristics of Trace Elements in $PM_{2.5}$ and PM_{10} of Chifeng, Northeast China, Insights into Spatiotemporal Variations and Sources. *Atmos. Res.* **2018**, *213*, 550–561. [CrossRef]

50. Yin, S.; Wang, X.; Zhang, X.; Zhang, Z.; Xiao, Y.; Tani, H.; Sun, Z. Exploring the Effects of Crop Residue Burning on Local Haze Pollution in Northeast China Using Ground and Satellite Data. *Atmos. Environ.* **2019**, *199*, 189–201. [CrossRef]

51. Zhao, H.; Che, H.; Zhang, L.; Gui, K.; Ma, Y.; Wang, Y.; Wang, H.; Zheng, Y.; Zhang, X. How Aerosol Transport from the North China Plain Contributes to Air Quality in Northeast China. *Sci. Total Environ.* **2020**, *738*, 139555. [CrossRef] [PubMed]

52. Yang, J.; Wang, J.; Xiao, X.; Jin, C.; Xia, J.; Li, X. Spatial Differentiation of Urban Wind and Thermal Environment in Different Grid Sizes. *Urban Clim.* **2019**, *28*, 100458. [CrossRef]

53. Zou, B.; Pu, Q.; Luo, Y.; Tian, Y.; Zhang, W. On the Complex Indicative System Based on the Spatially Divided Urban Areas for $PM_{2.5}$ Pollution & Control. *J. Saf. Environ.* **2016**, *16*, 342–347. (In Chinese)

54. Chai, M.; Wu, L.; Xiang, C.; Zou, B. Analysis of the Variation Characteristics of $PM_{2.5}$ Mass Concentration Around the Heating Period in the Central Liaoning Province. Environ. *Sci. Technol.* **2018**, *41*, 117–123. (In Chinese) [CrossRef]

55. Li, X.; Hu, X.; Ma, Y.; Wang, Y.; Li, L.; Zhao, Z. Impact of Planetary Boundary Layer Structure on the Formation and Evolution of Air-pollution Episodes in Shenyang; Northeast China. *Atmos. Environ.* **2019**, *214*, 116850. [CrossRef]

56. Yu, T.; Song, Y.; Hao, F. Space Pattern Evolution of Population Distribution and the Driving Factors in Northeast China. *Sci. Geogr. Sin.* **2017**, *37*, 709–717. (In Chinese) [CrossRef]

57. Carolien, B.; Panis, L.I.; Arentze, T.; Janssens, D.; Torfs, R.; Broekx, S.; Wets, G. A Dynamic Activity-based Population Modelling Approach to Evaluate Exposure to Air Pollution: Methods and Application to A Dutch Urban Area. *Environ. Impact. Assess. Rev.* **2009**, *29*, 179–185. [CrossRef]